Electronic structure of the cubic perovskite $SrMn_{1-x}Fe_xO_3$ investigated by x-ray spectroscopies

J.-S. Kang,[1,*] H. J. Lee,[1] G. Kim,[1] D. H. Kim,[1] B. Dabrowski,[2] S. Kolesnik,[2] Hangil Lee,[3] J.-Y. Kim,[3] and B. I. Min[4]
[1]*Department of Physics, The Catholic University of Korea (CUK), Bucheon 420-743, Republic of Korea*
[2]*Department of Physics, Northern Illinois University, DeKalb, Illinois 600115, USA*
[3]*Pohang Accelerator Laboratory (PAL), POSTECH, Pohang 790-784, Republic of Korea*
[4]*Department of Physics, POSTECH, Pohang 790-784, Republic of Korea*
(Received 5 May 2008; revised manuscript received 15 July 2008; published 21 August 2008)

The electronic structures of $SrMn_{1-x}Fe_xO_3$ ($0 \leq x \leq 1$) have been investigated by using photoemission spectroscopy (PES), soft x-ray absorption spectroscopy, and soft x-ray magnetic circular dichroism (XMCD). Both Mn and Fe ions are found to be nearly tetravalent for the whole range of x in $SrMn_{1-x}Fe_xO_3$. Valence-band PES measurements show the broader Fe $3d$ ($t_{2g}^3 e_g^1$) bands than the Mn $3d$ (t_{2g}^3) bands and the finite metallic intensity near E_F in the Fe $3d$ PES of $SrFeO_3$ in agreement with the metallic ground state of $SrFeO_3$. The Fe $2p$ XMCD spectra exhibit the enhanced XMCD effect for $0.6 \leq x \leq 0.8$ in $SrMn_{1-x}Fe_xO_3$, which is consistent with the spin-glass behavior in the intermediate substitution, while the Mn $2p$ states exhibit the negligible XMCD effect.

DOI: 10.1103/PhysRevB.78.054434 PACS number(s): 78.70.Dm, 79.60.−i, 87.64.ku, 74.25.Jb

Perovskite $SrFeO_3$ shows the metallic behavior when fully oxygenated.[1,2] $SrFeO_3$ exhibits neither the Jahn-Teller distortion[3,4] nor the orbital ordering,[5] which is unusual considering that high-spin (HS) Fe^{4+} ($t_{2g}^3 e_g^1$) ions are usually Jahn-Teller active. Oxygen deficiency in $SrFeO_{3-\delta}$ affects the transport properties dramatically, causing the metal-to-insulator transition (MIT) for $\delta \geq 0.15$.[4,6–9] It is likely that the MIT in $SrFeO_{3-\delta}$ is accompanied by the charge ordering of mixed-valent Fe^{3+}/Fe^{4+} ions. In this aspect, it is interesting to study $SrMn_{1-x}Fe_xO_3$ perovskite oxides, which are expected to exhibit competition between various valence states of Mn (3+ and 4+) and Fe (3+, 4+, and 5+). Since the $Fe^{4+}(3d^4)$ ion is isoelectronic with the $Mn^{3+}(3d^4)$ ion, $SrMn_{1-x}Fe_xO_3$ with $Mn^{4+}(t_{2g}^3)$ and $Fe^{4+}(t_{2g}^3 e_g^1)$ ions is expected to demonstrate the competing spin, charge, and lattice interactions similar to doped perovskite manganite oxides of $R_{1-x}A_xMnO_3$ [R=rare-earth ions and A=divalent ions (Ca, Sr, and Ba)], which in particular could lead to ferromagnetism and colossal magnetoresistance.

Both $SrMnO_3$ and $SrFeO_3$ show the antiferromagnetic (AF) ordering with Néel temperatures T_N=233 K for $SrMnO_3$ (Ref. 10) (G type) and T_N=134 K for $SrFeO_3$ (Ref. 11) (spiral type). On a substitution of the cubic perovskite $SrMnO_3$ preserving the valence state 4+ of Mn (e.g., $Sr_{1-y}Ca_yMnO_3$), the AF ordering is observed in the cubic, tetragonal, and orthorhombic crystal structures.[12] T_N is gradually suppressed by the deviation of the Mn-O-Mn bond angle from 180° and by the variance of the average size of the A-site ion via changes in the Sr/Ca ratio.[12,13] Cubic $SrMn_{1-x}Fe_xO_3$ with 180° bond angles shows rapid suppression of both the G- and spiral-type AF orders and exhibits the antiferromagnetic order and/or the spin-glass behavior at an intermediate substitution.[5] No ferromagnetism or magnetoresistance has been observed.

With the Mn substitution in $SrFeO_3$, the system becomes an insulator. Mössbauer measurements[5,14] for $SrMn_{1-x}Fe_xO_3$ revealed that there are two types of Fe ions for $x < 1$, which were considered to be in the charge disproportionation (CD) of $Fe^{3+}(d^5)+Fe^{5+}(d^3)$. Note that Mössbauer spectroscopy revealed no CD feature for metallic $SrFeO_3$.[5,15] For isoelectronic charge-ordered (CO) $CaFeO_3$, however, such a CD feature was observed in Mössbauer spectroscopy.[15] On the other hand, the analysis of x-ray photoemission spectra[16–18] suggested that the CO state in $CaFeO_3$ results from the CD of $2d^5\underline{L} \rightarrow d^5\underline{L}^2 + d^5$ rather than $2d^4 \rightarrow d^3 + d^5$ ($\underline{L}$; an oxygen hole or a ligand hole). Hence, a further study is needed to settle down the issue of Fe valence states in $SrMn_{1-x}Fe_xO_3$.

In order to better understand the peculiar electronic and magnetic properties of $SrMn_{1-x}Fe_xO_3$, it is essential to investigate the electronic structures of Fe and Mn $3d$ electrons. In this work, we have investigated the valence and spin states of Mn and Fe ions in stoichiometric $SrMn_{1-x}Fe_xO_3$ ($0 \leq x \leq 1$) by using photoemission spectroscopy (PES),[19] soft x-ray absorption spectroscopy (XAS),[20,21] and soft x-ray magnetic circular dichroism (XMCD).[22,23] These methods provide valuable information on the valence states and the electronic structures of solids.

Polycrystalline samples of $SrMn_{1-x}Fe_xO_3$ ($0 \leq x \leq 1$) were prepared by using a two-step synthesis methods as described in Ref. 5. X-ray powder-diffraction (XRD) and neutron powder-diffraction measurements revealed no impurity phase. PES, XAS, and XMCD experiments were performed at the 2A undulator beamlines of Pohang Accelerator Laboratory (PAL) at two different experimental chambers. The 2A beamline is an elliptically polarized undulator, from which the circularly polarized light was obtained with the degree of circular polarization of >90%. Samples were cleaned *in situ* by repeated scraping with a diamond file under the base pressure of $\sim 7 \times 10^{-11}$ Torr. The data presented in this paper were obtained from the samples nearly free of surface contamination. PES spectra were obtained at room temperature by using a SCIENTA SES100 analyzer. The Fermi level E_F and the overall energy resolution of the system [full width at half maximum (FWHM)] were determined from the Fermi-edge spectrum of scraped Au metal. The FWHM of the valence-band PES spectra was set at ~150 meV at $h\nu \sim 600$ eV. XAS spectra were obtained both at room temperature and at $T \sim 80$ K (Ref. 24) by employing the total electron yield

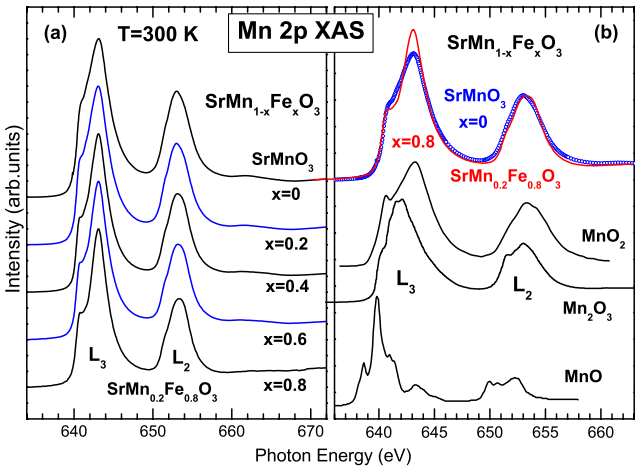

FIG. 1. (Color online) Comparison of the Mn $2p$ XAS spectra of $SrMn_{1-x}Fe_xO_3$ with those of MnO_2 (Mn^{4+}), Mn_2O_3 (Mn^{3+}), and MnO (Mn^{2+}).

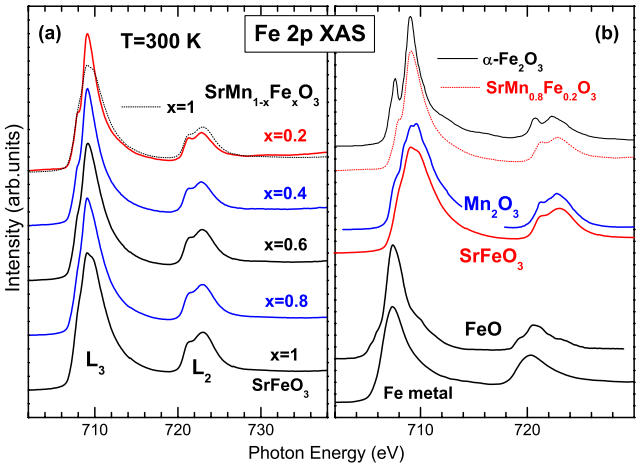

FIG. 2. (Color online) Comparison of the Fe $2p$ XAS spectra of $SrMn_{1-x}Fe_xO_3$ with those of Mn_2O_3 (Mn^{3+}:$3d^4$) and Fe_2O_3 (Fe^{3+}:$3d^5$). Here Mn_2O_3 ($3d^4$) is chosen to represent the isoelectronic Fe^{4+}($3d^4$) ion.

(TEY) mode with the photon energy resolution of ~100 meV at $h\nu \sim 700$ eV.

XMCD measurements were done at $T \sim 80$ K under the applied magnetic field of ~0.7 T. XMCD spectra were taken for a fixed helicity of light by reversing the applied magnetic field at each $h\nu$. In order to minimize the artificial effects caused by the decreasing photon flux with time, the direction of the applied magnetic field was reversed at each data point in the XMCD data acquisition. XMCD spectra were obtained by employing the TEY mode with the photon energy resolution of ~120 meV at $h\nu \sim 700$ eV. All the PES, XAS, and XMCD spectra were normalized to the incident photon flux.

Figure 1(a) shows the measured Mn $2p$ XAS spectra of $SrMn_{1-x}Fe_xO_3$ for $x=0$, 0.2, 0.4, 0.6, and 0.8. As the amount of substituted Fe increases, the energy positions of the L_3 ($2p_{3/2}$) and L_2 ($2p_{1/2}$) peaks do not change and their line shapes remain similar. These findings indicate that the valence state of Mn does not change with x. As x increases, the FWHM of the Mn L_3 peak decreases—resulting in the narrowing of the L_3 peak and, concomitantly, the more pronounced low-energy shoulder with increasing x ($h\nu$ ~641 eV). This trend is shown more clearly at the top of Fig. 1(b), where two XAS spectra of $x=0.8$ ($SrMn_{0.2}Fe_{0.8}O_3$) and $x=0$ ($SrMnO_3$) are scaled to have the same area. Also note that the intensities of the L_2 peaks of $x=0.8$ and 0 are almost the same in this scale. The more pronounced shoulder structure of the Mn L_3 peak with increasing x implies the weaker covalency of the Mn $3d$ orbitals in the dilute Mn concentration. The weaker covalency (the increased localized character) in the dilute Mn concentration could result in the reduction in the charge-transfer effect[21,25,26] between the Mn $3d$ orbitals and the O $2p$ ligand orbitals ($\underline{L}$) from $x=0$ to 0.8. This trend seems to be contrary to the more metallic nature of $SrMn_{1-x}Fe_xO_3$ for increasing x, and so the origin of the reduced charge-transfer effect for large x is not clear at the moment.

Figure 1(b) compares the Mn $2p$ XAS spectra of $SrMnO_3$ ($x=0$) and $SrMn_{0.2}Fe_{0.8}O_3$ ($x=0.8$) with those of reference oxides such as tetravalent MnO_2 (Mn^{4+}:$3d^3$),[27,28] trivalent Mn_2O_3 (Mn^{3+}),[28] and divalent MnO (Mn^{2+}:$3d^5$).[27] The peak positions and the line shapes of both $x=0$ and 0.8 are similar to those of MnO_2 but quite different from those of Mn_2O_3 and MnO, indicating that Mn ions are formally tetravalent (Mn^{4+}:$3d^3$) in the whole range of substitutions. Some differences between the Mn $2p$ XAS spectra of $SrMn_{1-x}Fe_xO_3$ and that of MnO_2 might be due to the different ligand fields and the different charge-transfer effects between $SrMnO_3$ and MnO_2. The nature of tetravalent Mn^{4+} states for all x in $SrMn_{1-x}Fe_xO_3$ is also supported by the negligible Mn $2p$ XMCD effect in $SrMn_{1-x}Fe_xO_3$ for all x values as shown in Fig. 5.

Figure 2(a) shows the measured Fe $2p$ XAS spectra of $SrMn_{1-x}Fe_xO_3$ for $x=0.2$, 0.4, 0.6, 0.8, and 1 and Fig. 2(b) compares the Fe $2p$ XAS spectra of $SrFeO_3$ with those of reference oxides for trivalent Fe_2O_3 (Fe^{3+}:$3d^5$),[29] divalent FeO (Fe^{2+}:$3d^6$),[29] and Fe metal.[30] In Fig. 2(b), we have chosen Mn_2O_3 (Ref. 28) to represent the tetravalent (Fe^{4+}) state because both of them are isoelectronic in the ground state with the $3d^4$ configuration (the L_3 and L_2 parts of the Mn_2O_3 spectrum have been separated and shifted to be aligned to the corresponding L_3 and L_2 peaks of $SrFeO_3$). The line shape of our Fe $2p$ XAS spectrum for $x=1$ ($SrFeO_3$) is similar to that in literature.[25,26,31]

It is clearly shown that the measured Fe $2p$ XAS spectrum of $SrFeO_3$ is very similar to that of Mn_2O_3 ($3d^4$) but different from those of α-Fe_2O_3 and Fe metal, providing evidence that Fe ions are formally tetravalent (Fe^{4+}) in $SrFeO_3$. This conclusion agrees with the interpretation of the Mössbauer spectrum for $SrFeO_3$ single crystal.[7] In contrast, two major discrepancies are observed clearly between $SrFeO_3$ and α-Fe_2O_3 with trivalent Fe ions. First, the low-energy peak (at ~707.6 eV) in α-Fe_2O_3 is missing in $SrFeO_3$. Second, the line shape of the L_2 peak for $SrFeO_3$ is different from that of α-Fe_2O_3. These discrepancies confirm that Fe ions are not trivalent in $SrFeO_3$. Note further that the line shape of the Fe $2p$ XAS of $SrFeO_3$ is very different from that of MnO_2 (Mn^{4+}:$3d^3$) [see Fig. 1(b)]. MnO_2 could be considered to represent the quintvalent Fe^{5+} state since Fe^{5+} and

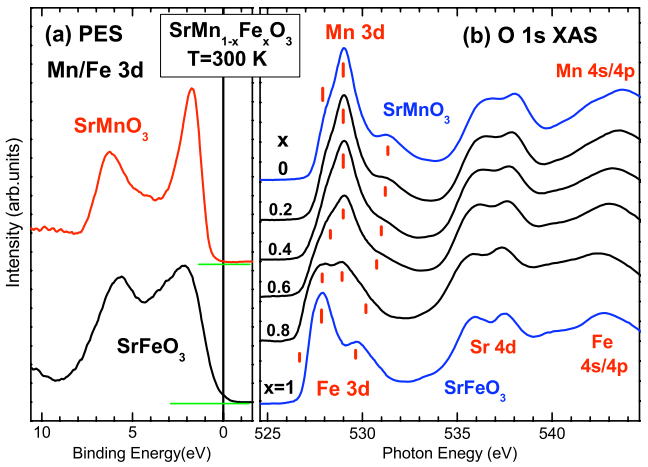

FIG. 3. (Color online) (a) Comparison of the valence-band PES spectra of $SrMn_{1-x}Fe_xO_3$ for $x=0$ and $x=1$. The Mn $3d$ and Fe $3d$ PES spectra represent the partial spectral weight distribution of the Mn and Fe $3d$ electrons, respectively. See the text for the details. (b) Comparison of the O $1s$ XAS spectra of $SrMn_{1-x}Fe_xO_3$. Each feature is identified in the figure. PES and O $1s$ XAS spectra were obtained at room temperature.

Mn^{4+} ions have the isoelectronic $3d^3$ configuration. These differences provide unambiguous evidence for the absence of either Fe^{3+} or Fe^{5+} ions in $SrFeO_3$.

As x increases in $SrMn_{1-x}Fe_xO_3$, the energy positions of the L_3 ($2p_{3/2}$) and L_2 ($2p_{1/2}$) peaks do not change and their line shapes are very similar to one another [see Fig. 2(a)]. In particular, the line shape of the L_2 peak does not change with x in $SrMn_{1-x}Fe_xO_3$, indicating that the valence state of Fe^{4+} ions remains unchanged with x. Even though the low-energy shoulder ($h\nu \sim 708$ eV) becomes more pronounced in the dilute Fe concentration ($x=0.2$), its position is different from that of α-Fe_2O_3 ($h\nu \sim 707.6$ eV) and the line shape of the L_2 peak is very different from that of α-Fe_2O_3. Thus, the existence of the trivalent Fe^{3+} states is refuted even in the dilute Fe concentration. This conclusion seems to disagree with the suggestion of a possible CD of Fe^{3+}-Fe^{5+} in $SrMn_{1-x}Fe_xO_3$,[5] which was based on Mössbauer measurements.

As observed for the Mn $2p$ XAS spectra, the Fe L_3 peak becomes narrower as the Fe concentration decreases but keeping the valence states of Fe ions more or less the same. The narrowing of the linewidth might reflect the change in charge transfer from the O $2p$ ligand orbitals to Fe $3d$ orbitals due to the weaker covalency of Fe $3d$ orbitals in the dilute Fe concentration. Then this feature is consistent with the occurrence of the MIT with decreasing x.

Figure 3 compares the partial spectral weight distributions of the Mn and Fe $3d$ states in the valence-band PES spectra ($x=0,1$) and the O $1s$ XAS spectra of $SrMn_{1-x}Fe_xO_3$ ($0 \leq x \leq 1$). The Fe and Mn $3d$ PES spectra were determined from the Fe and Mn $2p \rightarrow 3d$ resonant photoemission spectroscopy (RPES) measurements. It is well known that the $3d$ electron emissions of transition-metal (T) ions are enhanced in the T $2p \rightarrow 3d$ RPES.[32] We have adopted the extraction procedures for the Fe and Mn $3d$ PES spectra as described in Ref. 33 (see Fig. 5 in Ref. 33 and the related explanation therein).

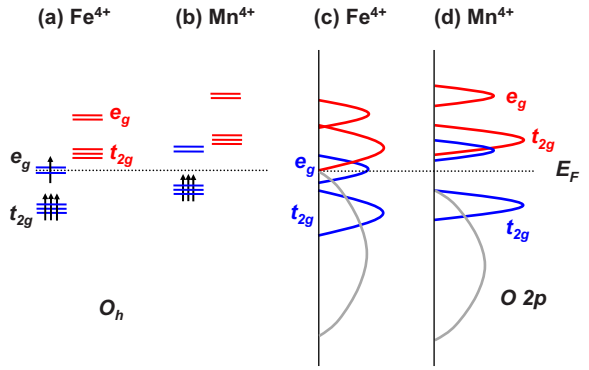

FIG. 4. (Color online) (a) and (b) The HS electronic configurations for a Fe^{4+} ion and Mn^{4+} ion, respectively, under the O_h symmetry. (c) and (d) Schematic PDOSs for Fe $3d$ and Mn $3d$ electrons in $SrMn_{1-x}Fe_xO_3$.

The Fermi level E_F in the valence-band PES spectrum corresponds to 0 eV in binding energy (BE). The Fe $3d$ PES spectrum of $SrFeO_3$ exhibits a rather broad peak centered at ~ 2 eV below E_F, while the Mn $3d$ PES spectrum of $SrMnO_3$ exhibits a sharp peak ~ 2 eV below E_F. Since Fe ions are tetravalent ($3d^4$) in $SrFeO_3$ (see Fig. 2), one can identify the broad peak (~ 2 eV BE) and the weak emission near E_F in $SrFeO_3$ as the occupied Fe $t_{2g}^3\uparrow$ and $e_g^1\uparrow$ states, respectively ($\uparrow$ denotes the majority spin). Similarly, the sharp peak at ~ 2 eV BE in $SrMnO_3$ is attributed to the occupied Mn $t_{2g}^3\uparrow$ states for $Mn^{4+}(3d^3)$ ions. The broad feature around 6–7 eV in BE for both $SrFeO_3$ and $SrMnO_3$ is considered to be the O $2p$ states that are hybridized with the Mn/Fe $3d$ states. The large O $2p$ electron character in Fe and Mn $3d$ PES spectra suggests the strong hybridization between Fe/Mn $3d$ and O $2p$ states in $SrMn_{1-x}Fe_xO_3$.

The O $1s$ XAS spectrum of a transition-metal oxide is considered to represent the unoccupied T $3d$, T sp, and Sr $4d$ states via the hybridization with the O $2p$ states.[34] The lowest-energy peaks in the O $1s$ XAS of $SrMn_{1-x}Fe_xO_3$ would correspond to the unoccupied $e_g\uparrow$ and $t_{2g}\downarrow$ states of Fe and Mn ions, while the shoulder at the higher-energy side would correspond to the unoccupied $e_g\downarrow$. Then the peaks at higher energies are attributed to the unoccupied Sr $4d$ and Fe/Mn $4s$-$4p$ states as labeled in Fig. 3(b) ($\downarrow$ denotes the minority spin). This figure reveals that the O $1s$ XAS spectra change systematically from $x=0$ to 1. Indeed the O $1s$ XAS spectra of the intermediate x concentrations can be reproduced by the linear combination of O $1s$ XAS spectra of $x=0$ and 1 even though the quantitative ratios of the two XAS spectra are not the same as the nominal concentrations of Fe and Mn ions in $SrMn_{1-x}Fe_xO_3$. More detailed assignments of these peaks are shown schematically in Fig. 4.

Note that the Fe $3d$ PES spectrum for $SrFeO_3$ reveals the finite spectral weight near E_F while that for $SrMnO_3$ reveals the negligible spectral weight near E_F. This trend agrees well with the metallic ground state of $SrFeO_3$ and the insulating ground state of $SrMnO_3$. The large-energy-scale line shapes of both the Mn $3d$ PES and the Fe $3d$ PES are found to be similar for the other x concentrations; and the finite spectral weights near E_F are observed for $x > \sim 0.6$ in the Fe $3d$ PES, while the spectral weights near E_F are negligible in the

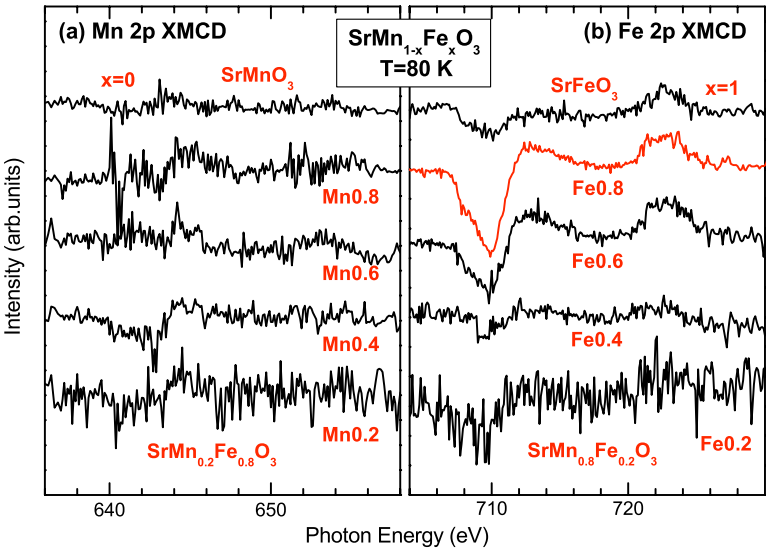

FIG. 5. (Color online) (a) Comparison of the Mn $2p$ XMCD spectra of $SrMn_{1-x}Fe_xO_3$. (b) Comparison of the Fe $2p$ XMCD spectra of $SrMn_{1-x}Fe_xO_3$. All the XMCD spectra were obtained at $T \sim 80$ K.

Mn $3d$ PES. Further, the broader Fe $3d$ PES peak—as compared to the Mn $3d$ PES peak—reflects the larger bandwidth of the Fe $3d$ states than the Mn $3d$ states. In other words, the Fe $3d$ electrons are more itinerant than the Mn $3d$ electrons, which is due to the stronger Fe $3d$-O $2p$ hybridization than the Mn $3d$-O $2p$ hybridization. The large Fe $3d$-O $2p$ covalency is consistent with the absence of the Jahn-Teller distortion in $SrFeO_3$. This conclusion is also consistent with the experimental signature of the increasing covalency of the Fe-O bond for larger x in $SrMn_{1-x}Fe_xO_3$, which was concluded from XRD measurements.[5]

In Figs. 4(a) and 4(b), we present the energy-level diagrams for Fe^{4+} and Mn^{4+} ions, respectively, based on the findings of Fig. 3. Here both Fe and Mn ions are under the O_h symmetry and assumed to have the HS electronic configurations. The corresponding schematic partial densities of states (PDOSs) for Fe $3d$ and Mn $3d$ electrons are shown in Figs. 4(c) and 4(d), respectively. Blue and red colors denote the majority-spin and minority-spin states, respectively. The essence of Fig. 4 is that both Fe and Mn ions are in the tetravalent states so that the topmost occupied states and the lowest unoccupied states are the Fe $e_g\uparrow$ states. Consequently, the lowest-energy peak of the O $1s$ XAS of $SrFeO_3$ is located closer to E_F than that of $SrMnO_3$ (see Fig. 3). This is because the unoccupied $e_g\uparrow$ majority-spin states of Fe^{4+} ions are partially filled, whereas the unoccupied $e_g\uparrow$ majority-spin states of Mn^{4+} ions are completely empty (well above E_F).

According to the above assignments, the exchange splitting energy J_H is roughly ~ 3 eV for both Fe^{4+} and Mn^{4+} ions, which is estimated from the energy separations between $e_g\uparrow$ (the lowest-energy peak) and $e_g\downarrow$ (the third peak) in the O $1s$ XAS. In the O $1s$ XAS, the energy separation between the second peak ($t_{2g}\downarrow$) and the third peak ($e_g\downarrow$) is roughly ~ 2 eV for both Fe and Mn ions, suggesting that the crystal-field energy 10Dq of Fe and Mn ions is about 10Dq ~ 2 eV.

Figure 5 compares the Mn and Fe $2p$ XMCD spectra of $SrMn_{1-x}Fe_xO_3$ ($0 \leq x \leq 1$). All the XMCD spectra have been normalized to the area of the corresponding XAS spectra. Our Fe $2p$ XMCD spectrum of $SrFeO_3$ is similar to that in literature,[31] even though the quality of our XMCD spectrum is worse probably due to the weaker magnetic field employed in this work (~ 0.7 T) than that in Ref. 31 (~ 2 T). The Mn $2p$ states in $SrMn_{1-x}Fe_xO_3$ exhibit essentially negligible XMCD effect for all x.

In contrast, the Fe $2p$ XMCD spectra of $SrMn_{1-x}Fe_xO_3$ show the enhanced XMCD signals for $0.6 \leq x \leq 0.8$, even though their absolute intensity is weak. This trend is shown better in Fig. 6, which plots the peak-to-peak intensity of the Fe L_3 ($2p_{3/2}$) XMCD spectra versus x in $SrMn_{1-x}Fe_xO_3$. In this figure, the Fe L_3 XMCD signal for each concentration is normalized to the integrated XAS intensity of the corresponding XAS spectrum, and the error bars represent the finite experimental errors in the estimation of the Fe L_3 XMCD signals. This finding is very interesting because the spin-glass behavior has been observed[5] in $SrMn_{1-x}Fe_xO_3$ for $0.6 \leq x \leq 0.8$. Our XMCD study suggests that the spin-glass behavior in $SrMn_{1-x}Fe_xO_3$ originates from Fe ions but not from Mn ions. Further, the finding of the essentially negligible XMCD effect for the Mn $2p$ states for all x supports the tetravalent Mn^{4+} states in $SrMn_{1-x}Fe_xO_3$, in agreement with that of Fig. 1.

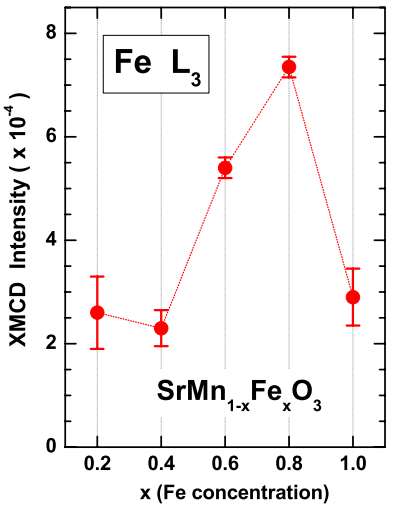

FIG. 6. (Color online) Plot of the peak-to-peak intensity of the Fe L_3 ($2p_{3/2}$) XMCD spectra versus x in $SrMn_{1-x}Fe_xO_3$. Error bars are denoted in this figure.

To summarize, the electronic structures of fully oxygenated $SrMn_{1-x}Fe_xO_3$ ($0 \leq x \leq 1$) have been investigated by using PES, XAS, and XMCD. XAS measurements near the Mn and Fe $2p$ absorption edges reveal that both Mn and Fe ions are nearly tetravalent in $SrMn_{1-x}Fe_xO_3$ for the whole range of x. Thus, no CD of $Fe^{3+}+Fe^{5+}$ is observed in $SrMn_{1-x}Fe_xO_3$ in this study. Valence-band PES reveals that the Mn^{4+} states with the $t_{2g}^3\uparrow$ occupied configuration are located about ~ 2 eV below E_F. On the other hand, the Fe $3d$ PES spectrum due to Fe^{4+} ($t_{2g}^3\uparrow e_g^1\uparrow$) states are broader than the Mn $3d$ PES spectrum. Further, the Fe $3d$ PES spectrum of $SrFeO_3$ exhibits the finite PES intensity near E_F. The latter finding agrees with the metallic ground state of $SrFeO_3$ and both of these findings indicate the stronger Fe $3d$-O $2p$ hybridization in $SrFeO_3$ than in $SrMnO_3$. The Fe $2p$ XMCD spectra for $SrMn_{1-x}Fe_xO_3$ exhibit the enhanced dichroic effect for $0.6 \leq x \leq 0.8$, which is consistent with the spin-glass behavior in magnetization measurements. In contrast, the Mn $2p$ states exhibit the negligible XMCD effect. Our finding in XMCD suggests the importance of Fe ions in determining the spin-glass behavior in $SrMn_{1-x}Fe_xO_3$.

This work was supported by the KRF (Grant No. KRF-2006-311-C00277), by the KOSEF through the eSSC at POSTECH, and in part by the 2008 Research Fund of the CUK. PAL is supported by the MOST and POSCO in Korea. Work at NIU was supported by the NSF (Grant No. DMR-0706610).

*Corresponding author. kangjs@catholic.ac.kr

[1] J. B. MacChesney, R. C. Sherwood, and J. F. Potter, J. Chem. Phys. **43**, 1907 (1965).
[2] H. Yamada, M. Kawasaki, and Y. Tokura, Appl. Phys. Lett. **80**, 622 (2002).
[3] H. Falcón, J. A. Barbero, J. A. Alonso, M. J. Martínez-Lope, and J. L. G. Fierro, Chem. Mater. **14**, 2325 (2002).
[4] P. Adler, A. Lebon, V. Damljanović, C. Ulrich, C. Bernhard, A. V. Boris, A. Maljuk, C. T. Lin, and B. Keimer, Phys. Rev. B **73**, 094451 (2006).
[5] S. Kolesnik, B. Dabrowski, J. Mais, D. E. Brown, R. Feng, O. Chmaissem, R. Kruk, and C. W. Kimball, Phys. Rev. B **67**, 144402 (2003).
[6] Y. M. Zhao and P. F. Zhou, J. Magn. Magn. Mater. **281**, 214 (2004).
[7] A. Lebon, P. Adler, C. Bernhard, A. V. Boris, A. V. Pimenov, A. Maljuk, C. T. Lin, C. Ulrich, and B. Keimer, Phys. Rev. Lett. **92**, 037202 (2004).
[8] S. Srinath, M. M. Kumar, M. L. Post, and H. Srikanth, Phys. Rev. B **72**, 054425 (2005).
[9] E. K. Hemery, G. V. M. Williams, and H. J. Trodahl, Phys. Rev. B **75**, 092403 (2007).
[10] T. Negas and R. S. Roth, J. Solid State Chem. **1**, 409 (1970).
[11] T. Takeda, Y. Yamaguchi, and H. Watanabe, J. Phys. Soc. Jpn. **33**, 967 (1972).
[12] O. Chmaissem, B. Dabrowski, S. Kolesnik, J. Mais, D. E. Brown, R. Kruk, P. Prior, B. Pyles, and J. D. Jorgensen, Phys. Rev. B **64**, 134412 (2001).
[13] B. Dabrowski, O. Chmaissem, J. Mais, S. Kolesnik, J. D. Jorgensen, and S. Short, J. Solid State Chem. **170**, 154 (2003).
[14] I. D. Fawcett, G. M. Veith, M. Greenblatt, M. Croft, and I. Nowik, Solid State Sci. **2**, 821 (2000).
[15] M. Takano, N. Nakanishi, Y. Takeda, S. Naka, and T. Takeda, Mater. Res. Bull. **12**, 923 (1977).
[16] A. E. Bocquet, A. Fujimori, T. Mizokawa, T. Saitoh, H. Namatame, S. Suga, N. Kimizuka, Y. Takeda, and M. Takano, Phys. Rev. B **45**, 1561 (1992).
[17] J. Matsuno, T. Mizokawa, A. Fujimori, Y. Takeda, S. Kawasaki, and M. Takano, Phys. Rev. B **66**, 193103 (2002).
[18] T. Akao, Y. Azuma, M. Usuda, Y. Nishihata, J. Mizuki, N. Hamada, N. Hayashi, T. Terashima, and M. Takano, Phys. Rev. Lett. **91**, 156405 (2003).
[19] S. Hüfner, in *Photoelectron Spectroscopy*, Solid-State Sciences Vol. 82 (Springer-Verlag, Berlin, 1995).
[20] F. M. F. de Groot, J. C. Fuggle, B. T. Thole, and G. A. Sawatzky, Phys. Rev. B **42**, 5459 (1990).
[21] G. van der Laan and I. W. Kirkman, J. Phys.: Condens. Matter **4**, 4189 (1992).
[22] B. T. Thole, P. Carra, F. Sette, and G. van der Laan, Phys. Rev. Lett. **68**, 1943 (1992).
[23] C. T. Chen, Y. U. Idzerda, H.-J. Lin, N. V. Smith, G. Meigs, E. Chaban, G. H. Ho, E. Pellegrin, and F. Sette, Phys. Rev. Lett. **75**, 152 (1995).
[24] The XAS spectra, obtained at room temperature and at $T \sim 80$ K, were essentially the same.
[25] M. Abbate, F. M. F. de Groot, J. C. Fuggle, A. Fujimori, O. Strebel, F. Lopez, M. Domke, G. Kaindl, G. A. Sawatzky, M. Takano, Y. Takeda, H. Eisaki, and S. Uchida, Phys. Rev. B **46**, 4511 (1992).
[26] M. Abbate, G. Zampieri, J. Okamoto, A. Fujimori, S. Kawasaki, and M. Takano, Phys. Rev. B **65**, 165120 (2002).
[27] C. Mitra, Z. Hu, P. Raychaudhuri, S. Wirth, S. I. Csiszar, H. H. Hsieh, H.-J. Lin, C. T. Chen, and L. H. Tjeng, Phys. Rev. B **67**, 092404 (2003).
[28] P. Ghigna, A. Campana, A. Lascialfari, A. Caneschi, D. Gatteschi, A. Tagliaferri, and F. Borgatti, Phys. Rev. B **64**, 132413 (2001).
[29] T. J. Regan, H. Ohldag, C. Stamm, F. Nolting, J. Lüning, J. Stöhr, and R. L. White, Phys. Rev. B **64**, 214422 (2001).
[30] J. S. Kang, G. Kim, H. J. Lee, D. H. Kim, H. S. Kim, J. H. Shim, S. Lee, H. G. Lee, J. Y. Kim, B. H. Kim, and B. I. Min, Phys. Rev. B **77**, 035121 (2008).
[31] J. Okamoto, K. Mamiya, S.-I. Fujimori, T. Okane, Y. Saitoh, Y. Muramatsu, K. Yoshii, A. Fujimori, A. Tanaka, M. Abbate, T. Koide, S. Ishiwata, S. Kawasaki, and M. Takano, Phys. Rev. B **71**, 104401 (2005).
[32] J. S. Kang, J. H. Kim, A. Sekiyama, S. Kasai, S. Suga, S. W. Han, K. H. Kim, E. J. Choi., T. Kimura, T. Muro, Y. Saitoh, C. G. Olson, J. H. Shim, and B. I. Min, Phys. Rev. B **68**, 012410 (2003).
[33] S. W. Han, J.-S. Kang, S. S. Lee, G. Kim, S. J. Kim, C. S. Kim, J.-Y. Kim, H. J. Shin, K. H. Kim, J. I. Jeong, B.-G. Park, J.-H. Park, and B. I. Min, J. Phys.: Condens. Matter **18**, 7413 (2006).
[34] J.-S. Kang, S. S. Lee, G. Kim, H. J. Lee, H. K. Song, Y. J. Shin, S. W. Han, C. Hwang, M. C. Jung, H. J. Shin, B. H. Kim, S. K. Kwon, and B. I. Min, Phys. Rev. B **76**, 195122 (2007).